Synthesis of Ultrafine SnO_{2-x} Nanocrystals by Pulsed Laser-Induced Reactive Quenching in Liquid Medium

Changhao Liang, Yoshiki Shimizu, Takeshi Sasaki, and Naoto Koshizaki*

Nanoarchitectonics Research Center (NARC), National Institute of Advanced Industrial Science and Technology (AIST), Central 5, 1-1-1 Higashi, Tsukuba, Ibaraki 305-8565, Japan

Received: March 24, 2003; In Final Form: June 20, 2003

We present the first synthesis of ultrafine tin oxide nanocrystals (2 to 3 nm) by pulsed laser ablation of a tin metal plate in aqueous solutions of sodium dodecyl sulfate (SDS) and in pure water. The particle size, phase structure, and surface states are characterized by X-ray diffraction (XRD), transmission electron microscopy (TEM), and X-ray photoelectron spectroscopy (XPS). Surfactant effects on the formation of tin oxide nanocrystals are also examined. Stable colloidal suspensions consisting of well-dispersed tin oxide nanocrystals with very narrow size distribution could be obtained with surfactant solution around the critical micelle concentration, and the formation of metal droplets was significantly suppressed. Optical transmittance spectrum analysis indicated that the optical gap of SnO_{2-x} nanocrystals increased to 3.81 eV with an average size of 2.5 nm due to quantum size effects. XPS investigation revealed that the valence of Sn in oxide nanoparticles surface is not four, but rather around three. A possible formation process of tin oxide is proposed based on laser-induced reactive quenching and surfactant-mediated growth. This unique technique could be extended to prepare other oxide nanocrystals.

Introduction

Ultrafine tin oxide nanocrystals are of great technological and scientific interest as a key functional material that is used extensively for photovoltaic devices,[1] transparent conductive electrodes,[2] and gas sensors.[3] Previous studies have demonstrated that the gas sensitivity of SnO_2 is greatly improved for particles smaller than 10 nm.[4] Crystalline SnO_2 is also a good candidate for wide-band-gap quantum dot systems since it has an energy gap of 3.6 eV,[5] an exciton binding energy of 32 meV,[5a] and an expected exciton Bohr radius of about 2.4 nm.[5a] Thus, fabrication of single-phase ultrafine SnO_2 nanocrystals with narrow size distribution is important for studies of their size-dependent electronic properties. Chemical methods such as sol−gel synthesis are commonly used to make fine-scale tin oxide nanoparticles.[6,7] However, freshly prepared tin oxide gel has a hydrous skeleton and is either amorphous or pseudocrystalline. Postfiring is therefore necessary, resulting in particle size increase and wider distribution.[8] Since particle growth is controlled by the motion of the boundaries between particles,[9] the inhibition of SnO_2 nanocrystal growth was recently implemented with addition of heterogeneous particles or in-situ secondary-phase particle generation, which resulted in interface poisoning. For example, Nb_2O_5 was doped to control the growth of SnO_2 by the polymeric precursor method,[10] $SrCO_3$ nanoparticles were added during calcination of hydrous SnO_2 nanoparticles,[11] extremely small SnO_2 nanoparticles were obtained during thermal oxidation of tin-doped silica xerogel,[12] and changing the hydroxyl group with the methylsiloxyl surface group before firing caused secondary phase "pinning" SiO_2 particles to form on the surface to prevent SnO_2 particle growth after decomposition.[8b]

We report here a new synthetic approach: pulsed laser ablation (PLA) of a pure metal plate in a liquid medium to directly produce ultrafine oxide nanocrystals without further heat treatment. Pulsed laser ablation is a unique method used to obtain atoms, ions, and small molecules from solid targets.[13] Most experiments on pulsed laser−solid interaction have been carried out in a vacuum or in diluted gases, aimed at thin film fabrication and cluster formation.[13,14] Only a few attempts have been made to produce new materials by PLA in a liquid medium employing the reaction between the ablated species and molecules in a liquid phase,[15] although this possibility was suggested in studies on laser ablation at solid−liquid interfaces.[16] Pulsed laser ablation in liquid has been primarily used to prepare metal nanoparticles since Henglein, Cotton, and their co-workers first developed this synthesis strategy.[17] Mafuné and co-workers examined the formation of gold and silver nanoparticles by laser ablation in the aqueous surfactants solutions.[18] Yeh and co-workers produced copper nanoparticles and gold−silver alloy nanoparticles in liquid media by laser ablation.[19] Laser irradiation has also been used to modify the size and shape of noble metal nanoparticles such as Ag and Au in colloidal solutions.[20] Interestingly, there have been few reports about synthesis of nanostructures using active main-group or transition-metal targets. Strong reactions may take place between the ablated species and encountered solution molecules such as water since the most nascent ablation species of active metal targets are electronically excited and hence highly reactive. Thus, ultrafine metal oxide nanoparticles are expected after rapid reactive quenching. The synthesized product is derived from its atomic constituents from the ablated solid and the participating liquid. We demonstrate the feasibility of this concept in this paper and present our experimental results on synthesis of SnO_{2-x} nanocrystals with a size comparable to its exciton radius by PLA of pure tin metal in pure water or in an aqueous solution of ionic surfactant. The surfactant is used to obtain stable monodisperse nanoparticles that are applicable for study of the optical and physicochemical properties in nanometer scale. Surfactant-

* Corresponding author. E-mail: koshizaki.naoto@aist.go.jp.

10.1021/jp0347466 CCC: $25.00
Published on Web 08/13/2003

covered water pools are known to provide unique microreactors for nucleation and growth of nanoparticles and further inhibit excess aggregation of particles through the attachment of hydrophilic headgroups on the surfaces of inorganic species.[21] We will also examine surfactant effects on the formation of oxide nanocrystals.

Experimental Section

Extremely fine tin oxide nanocrystals were produced through pulsed laser ablation of tin metal in pure water or in aqueous solutions of sodium dodecyl sulfate (SDS) surfactants with concentrations of 0.001 or 0.01 M. We refer to the products obtained from water, 0.001 M SDS, and 0.01 M SDS solutions as Samples A, B, and C. A tin metal plate (99.99%) was fixed on the bottom of a glass vessel filled with 7 cm^3 aqueous solution and was ablated with the third harmonic (355 nm) of a Nd:YAG laser operated at 10 Hz with a maximum output of 100 mJ/pulse. The laser beam was focused on a metal plate with a beam size of about 1 mm in diameter using a lens with a focal length of 250 mm. Laser ablation lasted for 60 min, and all solutions became slightly turbid but were still transparent after the ablation. There were a few cloud-like aggregates observed in the deionized water and many granular-like aggregates in the 0.001 M SDS solution (the aggregation in 0.001 M SDS solution was more severe than that in pure water). In contrast, the 0.01 M SDS solution was stable for more than one week without aggregation, and no obvious change of the corresponding optical spectrum was observed after one week. The optical transmittance spectra of the obtained colloidal solutions were recorded by a Shimadzu UV-2100 PC spectrometer with reference of corresponding original solutions to subtract the effects from solvents. All of the colloidal suspensions were repeatedly centrifuged at 5000 rpm, and the settled powder was washed with deionized water to remove as much SDS as possible. Small drops of the obtained concentrated suspensions were deposited on a carbon-coated copper grid for TEM/HRTEM observation, and others were transferred to a quartz substrate and dried in an air atmosphere to create a thin film at room temperature.

Results

X-ray powder diffraction (XRD) analysis of the collected products was performed using a powder Rigaku, RAD-C system with Cu Kα radiation ($\lambda = 1.54056$ Å, scanning rate 0.4°/min). Figure 1 depicts the XRD spectra of products collected from different solutions. The broad Bragg reflection peaks corresponded with the cassiterite structure of SnO_2 (JCPDS 77-0448), while the narrow sharp peaks agreed with the pure tin (Sn) phase (JSPDS 04-0673). The broad peaks indicate the formation of very small nanoparticles. Furthermore, the peak position and relative intensity indicate that an Sn phase formed in water and 0.001 M SDS solution, whereas nearly no Sn phase was observed in the 0.01 M SDS solution (despite the appearance of very weak Sn peaks). In contrast, nearly single phase tin oxide nanoparticles formed in 0.01 M SDS solution, while almost no crystalline tin oxide peaks appeared in Sample B. The surfactant concentration evidently plays a key role in the final phase constituents. The mean particle sizes from Samples A and C were estimated to be 2.69 and 2.37 nm using a (110) diffraction peak at 26.6° in 2θ based on Scherrer's equation.[22]

The particle size, distribution, and crystallinity were more directly investigated with a transmission electronic microscope (JEOL 2000FXII TEM and JEOL 2010 HRTEM). Low-magnification TEM observations indicated that tin oxide nanoparticles assembled into thin films on a carbon-coated grid, though it is difficult to distinguish single particles from each other (Figure 2). Selected area electron diffraction (SAED) analysis revealed that the particles from Samples A and C were

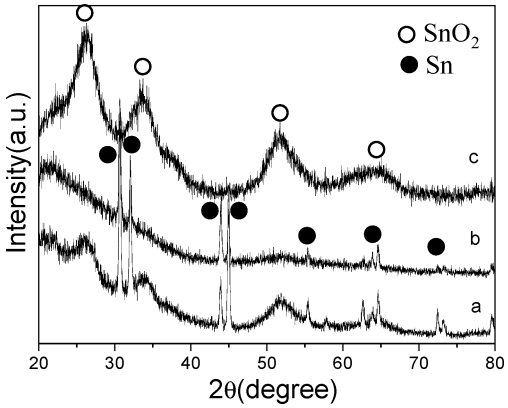

Figure 1. X-ray powder diffraction spectra of (a) sample A from Sn ablated in deionized water, (b) sample B from Sn ablated in 0.001 M SDS solution, and (c) sample C from Sn ablated in 0.01 M SDS solution. The broad peaks agree with cassiterite SnO_2, and the sharp peaks correspond to pure metal Sn.

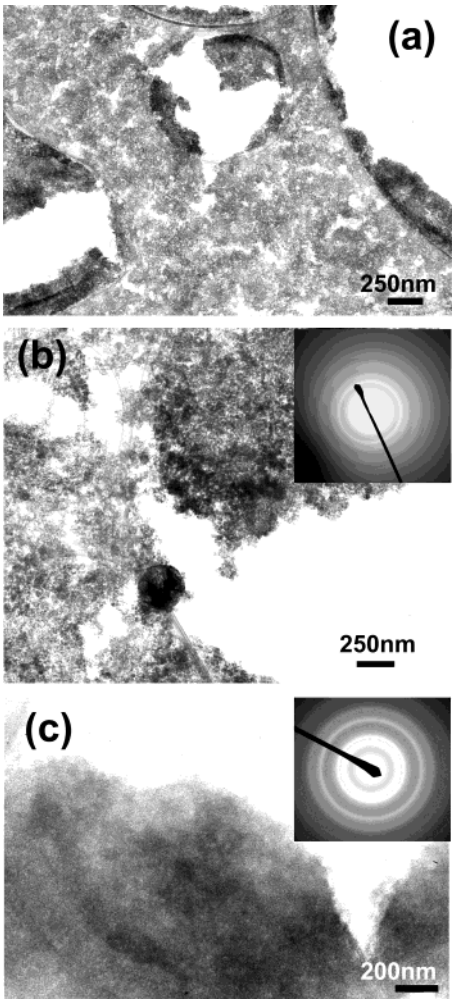

Figure 2. Low-magnification TEM images of tin oxide nanoparticles produced by pulsed laser ablation (a) in deionized water, (b) in 0.001 M SDS solution, and (c) in 0.01 M SDS solution. Insets depict the corresponding SAED patterns recorded from tin oxide nanoparticles (tin oxide nanoparticles in water exhibited a SAED pattern similar to that in Figure 2c). The larger round particle in Figure 2b corresponds to a tin metal droplet.

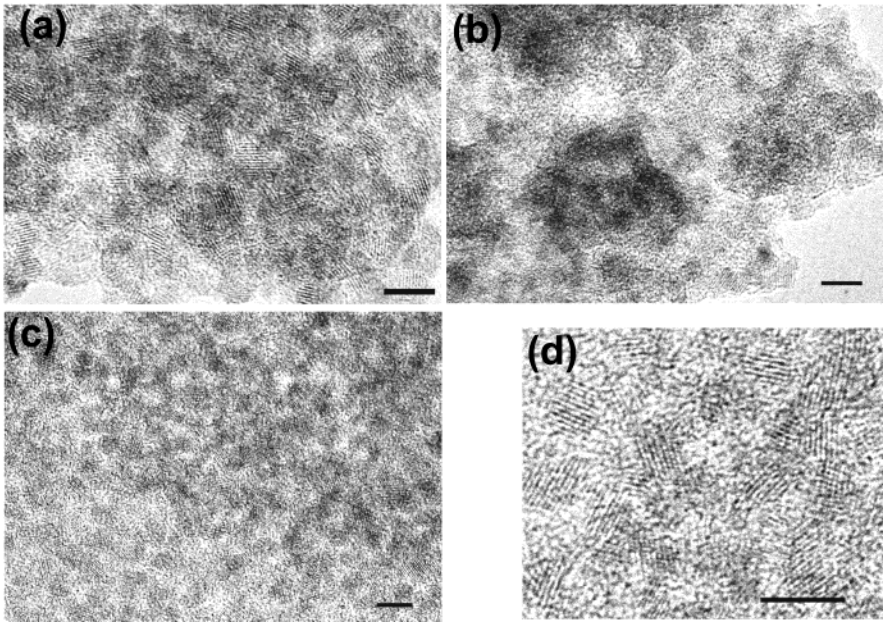

Figure 3. HRTEM images of tin oxide nanoparticles generated from different SDS solutions. (a) Sample A, (b) Sample B, (c) and (d) correspond to Sample C. All scale bars are 5 nm.

crystallized with bright polycrystalline diffraction rings (inset in Figure 2c), whereas the SAED pattern inset in Figure 2b indicates that many particles in Sample B were less crystallized. In addition, we observed some round tin droplet-like particles (100 to 200 nm in diameter) in Samples A and B (as illustrated in Figure 2b), but no metal droplets were observed in Sample C.

Figure 3 contains representative HRTEM images of nanoparticles from Samples A, B, and C. The particles were monodisperse and almost spheroid-shaped in Sample C, while many particles were connected without notable agglomeration in Sample A. A well-matched lattice between particles was also observed, indicating a possibly advanced stage of particle growth. Most importantly, the particle size distribution in Sample C was very narrow, while many particles in Sample A were not spheroid-shaped but rather exhibited an elongated shape. Measurement of about 75 nanoparticles from more HRTEM images indicated that the average particle diameter from Sample C was 2.5 ± 0.6 nm, which agrees with the XRD results, and that in Sample A was in a range of 2.5 to 4 nm. However, many agglomerated particles could be seen in Sample B, either in amorphous or crystalline state with clear lattice fringes, though the XRD spectrum of Sample B did not reflect any peak of crystallized tin oxide particles. The lattice spacing of these particles was well matched with the crystalline planes of cassiterite structure. Those randomly distributed tin oxide nanoparticles on the carbon-coated grid preferred a position with the {110} plane parallel to the incident electronic beam.

Figure 4 depicts the optical transmittance spectra recorded from colloidal solutions of Samples A, B, and C just after ablation. The sharp spectrum (c) with high absorbance in the UV region corresponds to stable colloidal suspensions of Sample C. Sample A also exhibited a sharp spectrum (a) but with lower transmittance, possibly due to the light scattering by dispersed tin metal particles and soft agglomerates. The broad spectrum (b) corresponds to colloidal suspensions of Sample B with severe agglomeration. These results combined with the above XRD and TEM investigations indicate that a stable colloidal suspension with monodispersed tin oxide nanocrystals could be produced by PLA of tin metal in a solution of 0.01 M SDS,

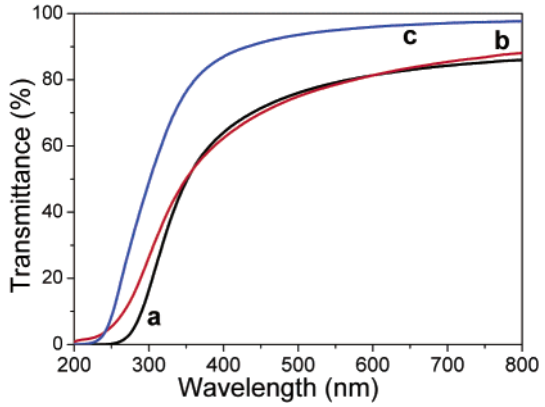

Figure 4. Optical transmittance spectra of tin oxide nanoparticles produced by laser ablation at 100 mJ/pulse in different solutions. (a) In deionized water (black), (b) in 0.001 M SDS solution (red), and (c) in 0.01 M SDS solution (blue).

and that crystalline nanoparticles produced in pure water are gradually aggregated. As stated previously, ultrafine SnO_2 nanocrystals with a size comparable to the exciton Bohr radius may have strong carrier confinement effects. We estimated the onset of absorption was obtained by extrapolating the steep linear part of the decreasing transmittance curve. The onset of absorption from Sample C was at $\lambda_{onset} = 325$ nm (3.81 eV). The optical-gap shift was about 0.21 eV with respect to the bulk band-gap of SnO_2 (3.6 eV). We used this energy shift of $\Delta E = 0.21$ eV to calculate the particle size (R) by means of a reported approximate expression [$\Delta E = (\hbar/2m_e^*)(\pi^2/R^2)$, where $\hbar$ is Planck's constant, m_e^* is the exciton reduced effective mass that may be replaced by the static electron effective mass m_e as $m_e^* = 0.27m_e \ll m_h$. Thus, the hole kinetic terms and corrections for the Coulomb interactions were ignored].[5,12] The calculated value of $R \approx 2.20$ nm was close to the average particle size estimated by TEM and XRD for Sample C. A similar analysis of the colloidal suspension from Sample A presented an onset of absorption at 333 nm (3.72 eV). Therefore, $\Delta E = 0.12$ eV corresponds to the calculated theoretical particle size 3.36 nm, which agrees with the HRTEM observation but is greater than

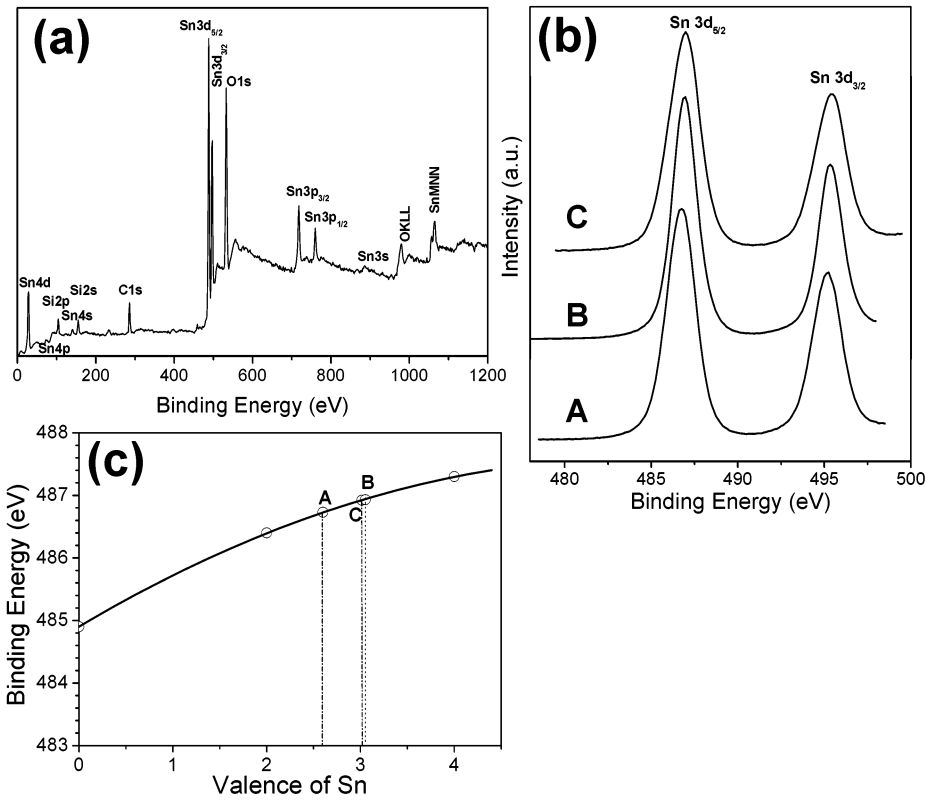

Figure 5. (a) X-ray photoelectron survey spectrum for Sample C, (b) Sn *3d* spectra from Samples A, B, and C, and (c) plot of the binding energies of Sn $3d_{5/2}$ in pure Sn, SnO, SnO_2, and tin oxide nanoparticles from Samples A, B, and C as a function of the Sn valence.

the size estimated from the XRD peak. This difference may come from the irregular shape of the particles in Sample A.

Recent studies[23] have indicated that the decrease in metal ion valence also contributes to blue shifts of the optical gap of tin oxide nanoparticles, but only to a small extent. We investigated the particle surface chemical states by XPS to clarify this point using PHI 5600ci. Figure 5a depicts the survey spectrum of tin oxide nanoparticles from colloidal suspensions in 0.01 M SDS solution (spectra from two other samples were similar). The figure clearly indicates that the photoelectron peaks of Sn, O, C, and weak Si peaks came from the quartz substrate. A carbon peak would be due to an adventitious contaminant and small traces of surfactant from Samples B and C, which can be separated by a Gaussian fit. The relative peak shifts due to the electrostatic charge-up were corrected by fixing the peak position of the contaminant carbon at 284.60 eV. The corrected XPS spectrum of O1s consisted of two separated peaks. The peak with binding energy around 530.8 eV corresponds to the Sn−O−Sn bonds, and the second weaker peak around 532 eV corresponds to hydroxyl bonds. Figure 4b provides the corrected XPS spectra of Sn 3*d* from different samples. We found that the Sn 3*d* peaks in all samples had only one component from tin oxide. No contribution from metal Sn was observed, though metal droplets were present in Samples A and B. We deduced that the surfaces of the round metal particles were most likely covered with smaller oxide nanoparticles. In fact, we observed this phenomenon in the TEM images. Figure 5c contains a plot of the binding energies of Sn $3d_{5/2}$ level vs the valences of Sn from pure Sn, SnO, and SnO_2.[24] The interpolated curve shown in Figure 5c and the binding energies of Sn $3d_{5/2}$ in Figure 5b led us to estimate the valences of Sn as 2.59 (Sample A), 3.05 (Sample B), and 3.02 (Sample C), all of which were much less than 4. However, the nanoparticles have the same structure as cassiterite SnO_2 from XRD analysis. This suggests that oxygen vacancies exist similar to the case reported in tin oxide films.[25] Therefore the obtained tin oxide nanoparticles are nonstoichiometric (SnO_{2-x}), with a number of oxygen vacancies near the surface of particles. In addition, the valence of Sn ions in Sample A is clearly lower than that in Sample C, but this difference has no apparent effect on the optical-gap blue shift in Sample A. Therefore, it is reasonable to conclude that the optical gap increase is mostly due to the size effects of monodispersed ultrafine crystalline SnO_{2-x} particles. Furthermore, the optical-gap change in our results differs significantly from previous results with an increased bang-gap of 3.97 eV to 3.5 nm SnO_2 nanocrystals that adsorbed onto the surface of $SrCO_3$ nanoparticles,[11] and no large blue shifts were observed in our quantum-sized SnO_{2-x} nanocrystals (e.g., in Sample C).

Discussion

The experimental results described above demonstrate that PLA of tin metal in liquid is an effective method to directly generate quantum-sized SnO_{2-x} nanocrystals. However, the fundamental mechanism regarding nanostructure formation by PLA in liquid is still not fully understood. In our experiments, we postulated a possible formation process of SnO_{2-x} nanoparticles based on laser-induced reactive quenching and surfactant-mediated growth. According to previous studies of laser ablation at liquid−solid interfaces, the initial stage of interaction between pulsed laser light and the target could create a plasma plume above the target surface. Since the plasma is confined in liquid in the pulse duration, it expands outside adiabatically at a supersonic velocity, thus creating a shock wave at the plasma−liquid interfaces, which induces extra pressure and further increases the plasma temperature.[26] The local higher pressure and temperature could promote impingement of ablated tin species into the liquid-confining plasma and subsequent chemi-

cal reaction. In our case, tin oxide clusters or particles would be formed by the reaction between active tin species and water molecules. A pH measurement revealed that the solution had changed from the initial neutral to an acidic state (4.5−5.3) after laser ablation, indicating the existence of hydrogen ions. We assume that the clusters or particles in this stage are insufficiently oxidized and crystallized due to transient reaction and rapid quenching. The formed clusters could be served as nuclei for further growth of SnO_{2-x} nanoparticles. In the following stage, our results demonstrated that surfactant molecules have played a key role in the aggregation and further crystallization of tin oxide clusters. First, due to insufficient oxidation (i.e., oxygen vacancies) and solutions in the acidic state (with ample H^+ ions), the tin oxide clusters formed are likely to be positively charged at the surface by reference of the isoelectric point of cassiterite SnO_2 (7.3).[27] The negatively charged $C_{12}H_{25}SO_4^-$ (DS^-) ions would preferably attach on the particle surface by electrostatic force. Obviously, surface coating is surfactant concentration dependent. In 0.01 M SDS solutions, we obtain a stable colloidal suspension of SnO_{2-x} nanoparticles with high crystallinity and maximum abundance, which was attributed to the formation a bilayer of DS^- coating on the particle surface in an aqueous solution of SDS around the critical micelle concentration (CMC) of SDS (8.6×10^{-3} M[28]).[29] In contrast, in lower concentration SDS solution (0.001 M), due to the incomplete coating, the tin oxide clusters were rapidly coagulated, and that the final particles are almost amorphous as revealed by XRD and TEM. However, in water, we still could obtain crystallized tin oxide particles but finally in the agglomerated state. This is because the repulsive force from surface charging could temporarily separate the clusters, which allows further oxidation and growth into crystalline particles by attachment of the hydroxyl groups or by a particle ripening process. The formed particles then agglomerate with the decrease in surface charging density.

However, it is difficult to fully understand why the SDS concentration around the CMC greatly suppresses the formation of tin droplets. TEM observations indicate that large round tin particles should directly result from melting of the target. We also carried out experiments using lower laser energy output, such as 80 and 50 mJ/pulse, in various solutions. The results indicated that lower laser energy has no effect on the final phase constituents, i.e., the maximum amount of tin droplets remained in the 0.001 M SDS solution and the formation of tin droplets was suppressed in the 0.01 M SDS solution with the maximum abundance of tin oxide nanocrystals. Correspondingly, the optical transmittance in the 0.01 M SDS solution was higher than that in water or in the 0.001 M SDS solution, as shown in Figure 4. Higher transmittance might effectively decompose ejected droplets by laser light, whereas lower transmittance and adsorption of agglomerated SnO_{2-x} on the droplets could inhibit the decomposition of droplets. The liquid environment in 0.01 M SDS solution may also constrain the ejection of droplets from the target. A better understanding of laser−solid interactions in liquid medium is required.

Summary

We demonstrated the possibility of one-step growth of quantum-sized tin oxide nanocrystals by PLA of pure active tin metal in a liquid medium. The liquid environment plays a crucial role in final particle size, distribution, and phase structure. We obtained stable colloidal suspensions consisting of SnO_{2-x} nanocrystals with maximum abundance in 0.01 M SDS solution. The size-dependent optical-gap shift was presented with an optical gap up to 3.81 eV, corresponding to an average particle size of 2.5 nm. A plausible process for the formation of SnO_{2-x} nanocrystals was proposed. We believe that this method is also applicable for synthesis of other metal oxide ultrafine nanocrystals.

Acknowledgment. C.H.L. acknowledges support from the Japan Society for the Promotion of Science (JSPS) fellowship at the National Institute of Advanced Industrial Science and Technology, Tsukuba, Japan.

References and Notes

(1) (a) Ferrere, S.; Zaban, A.; Gregg, B. A. *J. Phys. Chem. B* **1997**, 101, 4490. (b) Gaal, D. A.; Hupp, J. T. *J. Am. Chem. Soc.* **2000**, *122*, 10956.

(2) (a) Ginley, D. S.; Bright, C. *Mater. Res. Soc. Bull.* **2000**, *25*, 15. (b) Goebbert, C.; Agegerter, M. A.; Burgard, D.; Nass, R.; Schidt, H. *J. Mater. Chem.* **1999**, *9*, 253. (c) Cachet, H.; Bruneaux, J.; Folcher, G.; Lévy-Clément, C.; Vard, C.; Neumann-Spallart, M. *Sol. Energy Mater. Sol. Cells* **1997**, *46*, 101.

(3) (a) Sberveglieri, G. *Sens. Actuators B* **1992**, *6*, 239. (b) Martinelli, G.; Carotta, M. C.; Traversa, E.; Ghiotti, G. *Mater. Res. Soc. Bull.* **1999**, *24*, 30. (c) Robert, W. J. S.; Yang, S. M.; Chabanis, G.; Coombs, N.; Williams, D. E.; Ozin, G. A. *Adv. Mater.* **2001**, *13*, 1468. (d) Nayral, C.; Ould-Ely, T.; Maisonnat, A.; Chaudret, B.; Fau, P.; Lescouzères, L.; Peyre-Lavigne, A. *Adv. Mater.* **1999**, *11*, 61.

(4) Xu, C.; Tamaki, J.; Mirura, N.; Yamazoe, N. *Sens. Actuators B* **1991**, *3*, 147.

(5) (a) Agekyan, V. T. *Phys. Status Solidi A* **1977**, *43*, 11. (b) Summit, R.; Marley, J. A.; Borrelli, N. F. *J. Phys. Chem. Solids* **1964**, *25*, 1465.

(6) (a) Briois, V.; Santilli, C. V.; Pulcinelli, S. H.; Brito, G. E. S. *J. Non-Cryst. Solids* **1995**, *191*, 17. (b) Nutz, T.; Haase, M. *J. Phys. Chem B* **2000,** *104*, 8430. (c) Gamard, A.; Babot, O.; Jousseaume, B.; Rascle, M. C.; Toupance, T.; Campet, G. *Chem. Mater.* **2000**, *12*, 3419.

(7) Jolivet, J.-P. *Metal Oxide Chemistry and Synthesis: From Solution to Solid State*; Wiley-VCH: Weinheim, 2000.

(8) (a) Brinker C. J.; Scherer, G. W. *Sol−Gel Science: The Physics and Chemistry of Sol−Gel Processing*; Academic Press: San Diego, CA. 1990. (b) Wu, N. L.; Wang, S. Y.; Rusakova, I. A. *Science* **1999**, *285*, 1375.

(9) Chiang, Y.-M.; Birnie, D. P., III; Kingery, W. D. *Physical Ceramics−Principles for Ceramic Science and Engineering*; John Wiley & Sons: New York, 1997.

(10) Leite, E. R.; Weber, I. T.; Longo, E.; Varela, J. A. *Adv. Mater.* **2000**, *12*, 965.

(11) Pang, G. S.; Chen, S. G.; Koltypin, Y.; Zaban, A.; Feng, S. H.; Gedanken, A. *Nano Lett.* **2001**, *1*, 723.

(12) Chidini, N.; Paleari, A.; DiMartino, D.; Spinolo, G. *Appl. Phys. Lett.* **2002**, *81*, 1702.

(13) (a) Miller, J. C. *Laser Ablation: Principles and Applications*; Miller, J. C., Ed.; Springer-Verlag: Berlin, 1994; p 1. (b) Haglund, R. F., Jr.; Itoh, N. *Laser Abation: Principles and Applications*; Miller, J. C., Ed.; Springer-Verlag: Berlin, 1994; p 11.

(14) Chrisey, D. B.; Hubler, G. H. *Pulsed Laser Deposition of Thin Films*; Wiley-VCH: New York, 1994.

(15) (a) Ogale, S. B.; Patil, P. P.; Phase, D. M.; Bhandarkar, Y. V.; Kulkarni, S. K.; Kulkarni, S.; Ghaisas, S. V.; Kanetkar, S. M. *Phys. Rev. B* **1987**, *36*, 8237. (b) Lu, Y. F.; Huang, S. M.; Wang, X. B.; Shen, Z. X. *Appl. Phys. A: Mater. Sci. Process.* **1998**, *66*, 543. (c) Dolgaev, S. I.; Simakin, A. V.; Oronov, V. V.; Shafeev, G. A.; Bozon-Verduraz, F. *Appl. Surf. Sci.* **2002**, *186*, 546. (d) Yang, G. W.; Wang, J. B.; Liu, Q. X. *J. Phys. Condens. Matter* **1998**, *10*, 7923.

(16) (a) Sakka, T.; Iwanaga, S.; Ogata, Y. H.; Matsunawa, A.; Takemoto, T. *J. Chem. Phys.* **2000**, *112*, 8645. (b) Zhu, S.; Lu, Y. F.; Hong, M. H. *Appl. Phys. Lett.* **2001**, *79*, 1396.

(17) (a) Fojtik, A.; Henglein, A. *Ber. Bunsen-Ges. Phys. Chem.* **1993**, *97*, 252. (b) Neddersen, J.; Chumanov, G.; Cotton, T. M. *Appl. Spectrosc.* **1993**, *47*, 1959. (c) Sibbald, M. S.; Chumanov, G.; Cotton, T. M. *J. Phys. Chem.* **1996**, *100*, 4672.

(18) (a) Mafuné, F.; Kohno, J.; Takeda, Y.; Kondow, T.; Sawabe, H. *J. Phys. Chem. B* **2000**, *104*, 8333. (b) Mafuné, F.; Kohno, J.; Takeda, Y.; Kondow, T.; Sawabe, H. *J. Phys. Chem. B* **2000**, *104*, 9111. (c) Mafuné, F.; Kohno, J.; Takeda, Y.; Kondow, T.; Sawabe, H. *J. Phys. Chem. B* **2001**, *105*, 5114.

(19) (a) Yeh, M. S.; Yang, Y. S.; Lee, Y. P.; Lee, H. F.; Yeh, Y. H.; Yeh, C. S. *J. Phys. Chem. B* **1999**, *103*, 6851. (b) Chen, Y. H.; Yeh, C. S. *Chem. Commun.* **2001**, *4*, 371.

(20) (a) Kamat, P. V.; Flumiani, M.; Hartland, G. V. *J. Phys. Chem. B* **1998**, *102*, 3123. (b) Takami, A.; Kurita, H.; Koda, S. *J. Phys. Chem. B*

1999, *103*, 1226. (c) Lin, S.; Burda, C.; Mohamed, M. B.; Nikoobakht, B.; El-Sayed, M. A. *J. Phys. Chem. B* **2000,** *104*, 6152.

(21) Dixit, S. G.; Mahadeshwar, A. R.; Haram, S. K. *Colloid Surf. A* **1998**, *133*, 69.

(22) Jenkins, R.; Snyder, R. L. *Introduction to X-ray Powder Diffractometry*; John Wiley & Sons: New York, 1996; p 90.

(23) Tsunekawa, S.; Kang, J. Y.; Asami, K.; Kasuya, A. *J. Appl. Phys*. **2002**, *91*, 10098.

(24) Wang, D. N.; Miller, A. C. Notis, M. R. *Surf. Interface Anal*. **1996**, *24*, 127.

(25) Kaito, C.; Saito, Y. *J. Cryst. Growth* **1986**, *79*, 403.

(26) (a) Ageev, V. V.; Bokhonov, A. F.; Zhukovskii, V. V.; Yankovskii, A. A. *J. Appl. Spectrosc*. **1997**, *64*, 683. (b) Berthe, L.; Fabbro, R.; Peyre, P.; Tollier, L.; Bartnicki, E. *J. Appl. Phys*. **1997**, *82*, 2826. (c) Zhu, S.; Lu, Y. F.; Hong, M. H.; Chen, X. Y. *J. Appl. Phys*. **2001**, *89*, 2400.

(27) Parks, G. A. *Chem. Rev*. **1965**, *65*, 177.

(28) Fuerstnau, D. W. *J. Colloid Interface Sci*. **2002**, *256*, 79.

(29) (a) Matijević, E.; Ottewill, R. H. *J. Colloid. Sci*. **1958**, *13*, 242. (b) Ogihara, K. Tomioka, S.; Esumi, K.; Meguro, K. *J. Jpn. Soc. Color Mater*. **1982**, *55*, 546. (c) Esumi, K. *J. Colloid Interface Sci*. **2001**, *241*, 1.